

Uni3R: Unified 3D Reconstruction and Semantic Understanding via Generalizable Gaussian Splatting from Unposed Multi-View Images

Xiangyu Sun^{1*} Haoyi Jiang^{2‡} Liu Liu^{4‡} Seungtae Nam³ Gyeongjin Kang¹
Xinjie Wang⁴ Wei Sui⁵ Zhizhong Su⁴ Wenyu Liu² Xinggang Wang² Eunbyung Park^{3§}

¹Sungkyunkwan University ²Huazhong University of Science & Technology

³Yonsei University ⁴Horizon Robotics ⁵D-Robotics

https://horizonrobotics.github.io/robot_lab/uni3R/

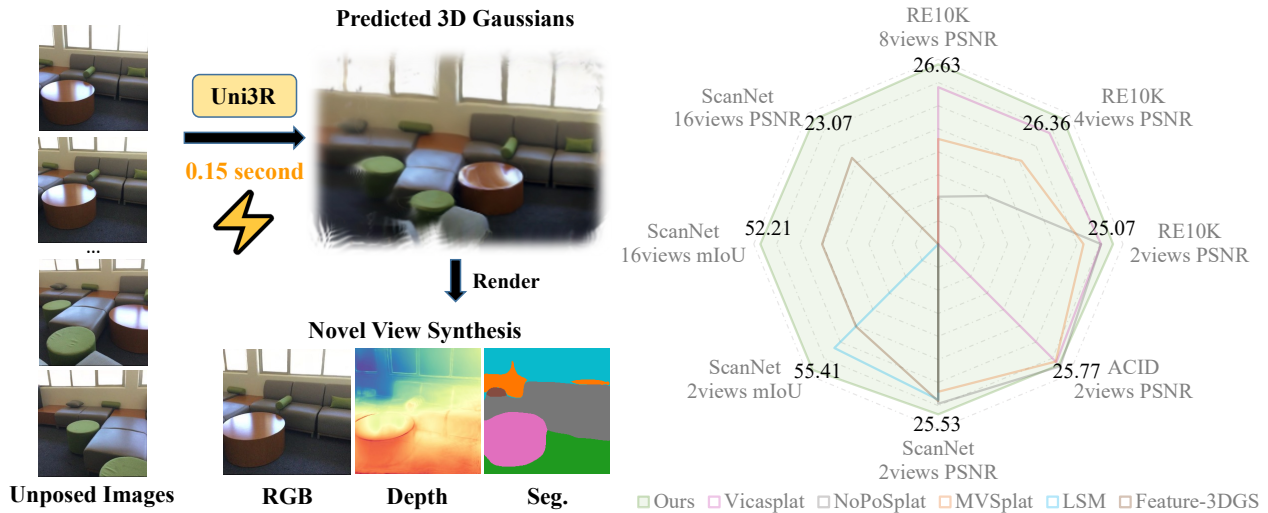


Figure 1. Uni3R takes unposed arbitrary multi-view images as input and produces a unified 3D Gaussian scene representation, enabling state-of-the-art performance in view synthesis, semantic segmentation, and depth estimation within a single forward pass.

Abstract

Reconstructing and semantically interpreting 3D scenes from sparse 2D views remains a fundamental challenge in computer vision. Conventional methods often decouple semantic understanding from reconstruction or necessitate costly per-scene optimization, thereby restricting their scalability and generalizability. In this paper, we introduce **Uni3R**, a novel feed-forward framework that jointly reconstructs a unified 3D scene representation enriched with open-vocabulary semantics, directly from unposed multi-view images. Our approach leverages a Cross-View Transformer to robustly integrate information across arbitrary

multi-view inputs, which then regresses a set of 3D Gaussian primitives endowed with semantic feature fields. This unified representation facilitates high-fidelity novel view synthesis, open-vocabulary 3D semantic segmentation, and depth prediction—all within a single, feed-forward pass. Extensive experiments demonstrate that Uni3R sets a new state of the art across multiple benchmarks, including in-domain datasets such as RE10K and ScanNet, as well as the out-of-domain dataset Mip-NeRF360. This work represents a new paradigm toward generalizable and unified 3D scene reconstruction and understanding.

1. Introduction

The ability to perceive and interpret the 3D world from sparse images is a cornerstone of computer vision, holding profound implications for robotics, autonomous driving, and augmented reality. While significant progress has been

*Equal contribution. Intern at Horizon Robotics

†Equal contribution. Intern at D-Robotics

‡Project leader

§Corresponding author

made in 3D reconstruction, led by photorealistic methods such as Neural Radiance Fields (NeRF) [24], 3D Gaussian Splatting (3DGS) [14], their reliance on time-consuming, per-scene optimization critically limits their generalizability to novel scenes. In response, a prominent class of generalizable 3D reconstruction methods [3, 5, 23, 39, 42] has emerged, which learn geometric priors across diverse scenes to perform feed-forward 3D reconstruction in a feed-forward manner.

While promising, these methods typically focus exclusively on geometry and appearance, overlooking the semantic richness crucial for holistic scene understanding. Recent efforts, including LangSplat [28] and Feature-3DGS [45], have incorporated semantic fields into 3D Gaussian Splatting, yet remain constrained by scene-specific optimization and lack scalability in real-world, zero-shot applications. More recently, approaches such as LSM [8] and UniForward [34] have aimed to unify semantic and radiance fields to jointly infer geometry, appearance, and semantics. However, these methods are built upon DUST3R [37], which is inherently designed for two-view inputs. Consequently, extending them to multi-view scenarios requires expensive pairwise feature matching across views, compromising efficiency and leading to inconsistent reconstructions due to the absence of global 3D context.

To address these limitations, we propose Uni3R, a novel, generalizable framework that synthesizes a unified 3D representation from arbitrary multi-view images for both high-fidelity rendering and dense, open-vocabulary semantic understanding. Leveraging a Cross-View Transformer effectively fuses information across views and produces globally consistent representations, Uni3R predicts unified 3D Gaussian primitives enriched with open-vocabulary semantic features. These Gaussian representations can be seamlessly rendered in real-time to synthesize novel views, supervised solely with source images and bypassing the need for per-scene optimization. Simultaneously, the embedded semantic features enable zero-shot 3D semantic segmentation by querying the scene with arbitrary text prompts.

To further enhance both geometric fidelity and training stability, we introduce a point-map-guided geometric loss that serves two key purposes. First, it enforces structural consistency and improves geometric accuracy, as evidenced by lower depth errors (e.g., AbsRel). Second, it stabilizes training by preventing the model from getting trapped in local minima when predicting the freedom 3D point distribution. Specifically, we employ a frozen VGGT [36] to generate dense point maps with associated confidence scores, which act as soft geometric priors to guide the spatial distribution of the 3D Gaussians.

Our contributions are summarized as follows:

- We introduce Uni3R, a novel feed-forward architecture that unifies 3D reconstruction and semantic understand-

ing. It predicts a set of Gaussian primitives with jointly integrated geometry, appearance, and open-vocabulary semantics in a single pass, eliminating the need for per-scene optimization.

- We demonstrate that a powerful geometry foundation model can be effectively extended beyond geometric estimation to support both photometric reconstruction and 3D scene understanding. Its cross-frame attention mechanism enables robust feature fusion to produce globally consistent scene representations from an arbitrary number of input views, while its predicted point maps provide potent geometric guidance.
- Uni3R achieves state-of-the-art performance across multiple tasks, including novel view synthesis, open-vocabulary 3D semantic segmentation, and depth prediction on the challenging RE10K [46] and ScanNet [6] datasets, underscoring its superior generalization and versatility.

2. Related Work

2.1. Differentiable Neural Representations

Traditional 3D reconstruction methods, such as Structure-from-Motion (SfM) [7] and Multi-View Stereo (MVS) [2] decompose the process into sequential steps, including feature matching, camera pose estimation, and geometric reconstruction. While effective, these multi-stage processes can be fragile and prone to error accumulation. The advent of Neural Radiance Fields (NeRF) [24] revolutionized novel view synthesis by introducing an end-to-end, differentiable approach that models a scene as a continuous function mapping 5D coordinates to color and volumetric density. More recently, 3D Gaussian Splatting (3DGS) [9, 14, 16, 33] has emerged as a compelling alternative, representing scenes explicitly with a set of 3D Gaussian primitives. Leveraging a highly efficient differentiable rasterizer, 3DGS supports real-time rendering speeds while maintaining exceptional rendering quality. However, canonical 3DGS relies on point clouds from SfM for initialization and rectified camera poses. Our work builds upon the 3DGS formulation but removes reliance on external tools like COLMAP [7]. By predicting Gaussians in an end-to-end pose-free manner, we enable scalable 3D reconstruction and scene understanding.

2.2. Feed-forward 3D Reconstruction

The substantial computational cost of per-scene optimization has motivated the development of 3D feed-forward models. PixelNeRF [42] and MVSNerf [4] learn scene priors across a large number of training scenes, enabling them to predict radiance fields for novel scenes from only a few input views. Following the success of 3DGS, pixelSplat [3], MVSplat [5], Generative Densification [25],

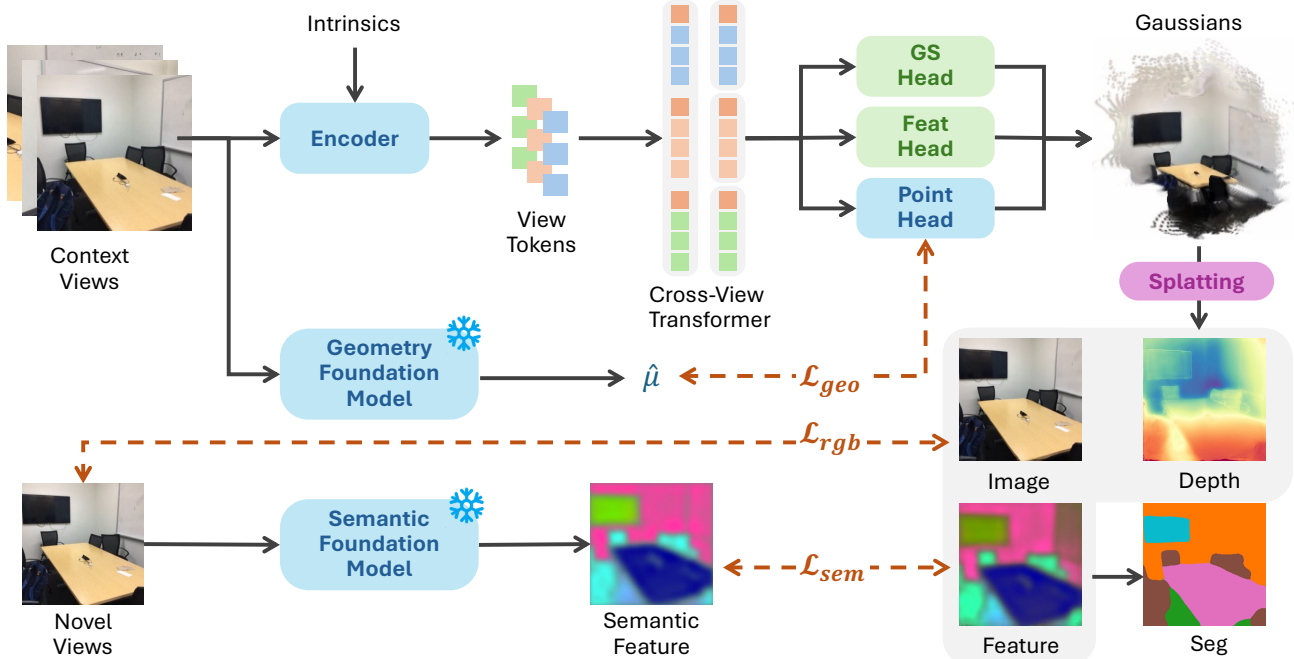


Figure 2. Architectural overview of the Uni3R pipeline. Uni3R predicts a set of Gaussian primitives with jointly integrated geometry, appearance, and open-vocabulary semantics in a single pass, eliminating the need for per-scene optimization.

iLRM [13] and DepthSplat [39] adapt this generalizable paradigm to predict 3D Gaussian parameters directly. However, these approaches typically necessitate known camera poses to guide the reconstruction. To eliminate this constraint, MAST3R [17] and DUST3R [37] demonstrate the feasibility of predicting pixel-aligned 3D point clouds directly from image pairs without explicit pose information. Building on these advances, Splatt3R [32] and NoPoSplat [40] further advance this pose-free paradigm by predicting 3D Gaussian primitives directly from image pairs. Despite their progress, models based on the DUST3R architecture still require sufficient overlap between image pairs and struggle to integrate globally consistent information, leading to fragmented reconstructions. Uni3R overcomes these limitations by employing a Cross-View Transformer, inspired by VGGT [36], to interpret and fuse information from an arbitrary number of views. Based on the globally consistent 3D geometric features, we develop a multi-view, pose-free feed-forward reconstruction model. Our method supports not only image pairs but also extended sequences or video clips, predicting 3D Gaussian primitives in a single forward pass to achieve high-quality, globally coherent 3D reconstruction without requiring camera poses.

2.3. Open-Vocabulary Segmentation in 3DGS

Integrating semantics into 3D reconstructions is crucial for higher-level scene understanding tasks. Early methods for 3D semantic segmentation required dense, 3D ground-truth labels, which are scarce and laborious to acquire. The ad-

vent of powerful 2D vision-language models like CLIP [19, 29] has spurred the development of open-vocabulary methods that lift 2D understanding into 3D. LERF [15] distills 2D CLIP features into 3D radiance fields. Capitalizing on the rendering efficiency of 3D Gaussian Splatting, several methods [21, 28, 43, 45] have extended Gaussian representations with semantic features. Nonetheless, these methods still rely on per-scene optimization, making them unsuitable for real-time applications in novel environments. While generalizable approaches like LSM [8] and GSemSplat [38] have been proposed, they are typically constrained to two-view inputs, restricting their scalability and robustness in complex scenes. In a related vein, GaussTR [11] explores generalizable Gaussian-based segmentation in the context of occupancy prediction. In contrast, Uni3R integrates open-vocabulary understanding into a generalizable, multi-view framework, producing globally consistent 3D representation embedded with expressive semantics without requiring any 3D semantic labels.

3. Method

This section details our methodology, beginning with the Feed-Forward 3D Gaussian Model in Sec. 3.1. We then describe how to endow Gaussians with semantics in Sec. 3.2, and conclude with the specifics of the training losses in Sec. 3.3, including photometric loss, semantic loss and geometry loss.

3.1. Feed-Forward Gaussian Splatting

3.1.1. Intrinsic Embedding

To resolve the inherent scale ambiguity in monocular reconstruction caused by unknown focal lengths, we incorporate an intrinsic embedding to provide essential geometric cues. Following NoPoSplat [40], we encode each camera’s focal length and principal point with a linear projection. The resulting intrinsic embedding is concatenated channel-wise with the corresponding image before patch tokenization, allowing the network to reason about the geometry-aware information.

3.1.2. Cross-View Transformer Encoder

Uni3R employs a Cross-View Transformer Encoder, following VGGT, to extract and fuse features from all input images into a consistent, view-agnostic latent representation. Each input view $I^{(i)}$, augmented with its intrinsic embedding, is first processed by a pre-trained Vision Transformer, DINOv2 [26], to extract a sequence of patch-level feature tokens. To support arbitrary multi-view inputs while maintaining permutation equivariance, a learnable camera token is appended to each view’s token sequence. The Cross-View Transformer Encoder consists of a series of Transformer blocks that alternate between intra-frame and cross-frame attention. Intra-frame self-attention operates within each view’s token set, refining the per-view features with local context. Subsequently, cross-frame global attention aggregates tokens from all views to establish correspondences and reason about the global 3D geometry. The output latent tokens from the encoder encapsulate a holistic and globally consistent understanding of the 3D scene.

3.1.3. Decoding Gaussian Parameters

The fused latent representations are decoded into a dense set of 3D Gaussian primitives with a Dense Prediction Transformer (DPT) [30] followed by dedicated prediction heads for different Gaussian parameters. DPT progressively refines coarse patch-level features with fine-grained local details from intermediate layers, yielding a dense per-pixel feature map.

Subsequently, we predict the properties of a set of pixel-aligned 3D Gaussians with separate MLP heads. Each primitive is parameterized by:

$$G_j = \{\mu_j, \alpha_j, c_j, s_j, r_j, f_j^{\text{sem}}\}, \quad (1)$$

where $\mu_j \in \mathbb{R}^3$ denotes the 3D center point, $s_j \in \mathbb{R}^3$ is the scale, $r_j \in \mathbb{R}^4$ is the rotation quaternion, $\alpha_j \in [0, 1]$ is the opacity, $c_j \in \mathbb{R}^3$ is the color, and $f_j^{\text{sem}} \in \mathbb{R}^d$ is a high-dimensional semantic feature vector.

The point head is initialized from pre-trained VGGT weights and is further fine-tuned with rendering-based supervision to align with real-world metric scales. Distinct

activation functions are applied to the predicted parameters to constrain them to their valid ranges:

$$\alpha_j = \sigma(f_j^\alpha), \quad (2)$$

$$s_j = \exp(f_j^s) \cdot d_{\text{median}}, \quad (3)$$

$$r_j = \text{normalize}(f_j^r), \quad (4)$$

where $\sigma(\cdot)$ represents the sigmoid activation function, and f_j^α , f_j^s , and f_j^r are the latents for opacity, scale, and rotation, respectively. The term d_{median} is the median depth value computed from the predicted 3D positions, which helps to normalize the scale.

3.2. Rendering with Open-Vocabulary Semantics

Once predicted, the set of Gaussians is rendered into novel views using the differentiable 3D Gaussian rasterizer, extended with semantic feature fields. The Gaussian function is described by:

$$G_j(x) = e^{-\frac{1}{2}x^\top \Sigma_j^{-1}x}, \quad (5)$$

where the covariance matrix Σ_j is constructed from the scale s_j and rotation r_j . The rendered color \hat{I} and feature \hat{F} at each pixel are computed by alpha-blending the properties of all sorted Gaussians that overlap it, taking \hat{F} as an example:

$$\hat{F} = \sum_i \hat{f}_i^{\text{sem}} \alpha_i \prod_{j=1}^{i-1} (1 - \alpha_j), \quad (6)$$

where \hat{f}_j^{sem} is compressed from f_j^{sem} by an autoencoder to mitigate the high memory cost of rendering high-dimensional semantic features.

$$\hat{f}_j^{\text{sem}} = \mathcal{F}_{\text{enc}}(f_j^{\text{sem}}), \quad (7)$$

$$\hat{F}' = \mathcal{F}_{\text{dec}}(\hat{F}), \quad (8)$$

where \mathcal{F}_{enc} and \mathcal{F}_{dec} are the encoder and decoder, respectively. The autoencoder is trained end-to-end to align the rendered features with CLIP-based image features, enabling efficient open-vocabulary semantic reasoning.

During inference, semantic segmentation is performed by computing the cosine similarity between the pixel-wise semantic features and a set of text-derived prototypes. Given a set of text prompts for desired categories (e.g., “wall,” “chair,” “sofa”), CLIP text encoder generates corresponding feature prototypes $f^{\text{txt}} \in \mathbb{R}^{N_C \times C}$, where N_C is the number of categories. The semantic logits S is then computed by cosine similarity:

$$S_p = \text{softmax}(f^{\text{txt}} \cdot \hat{F}'). \quad (9)$$

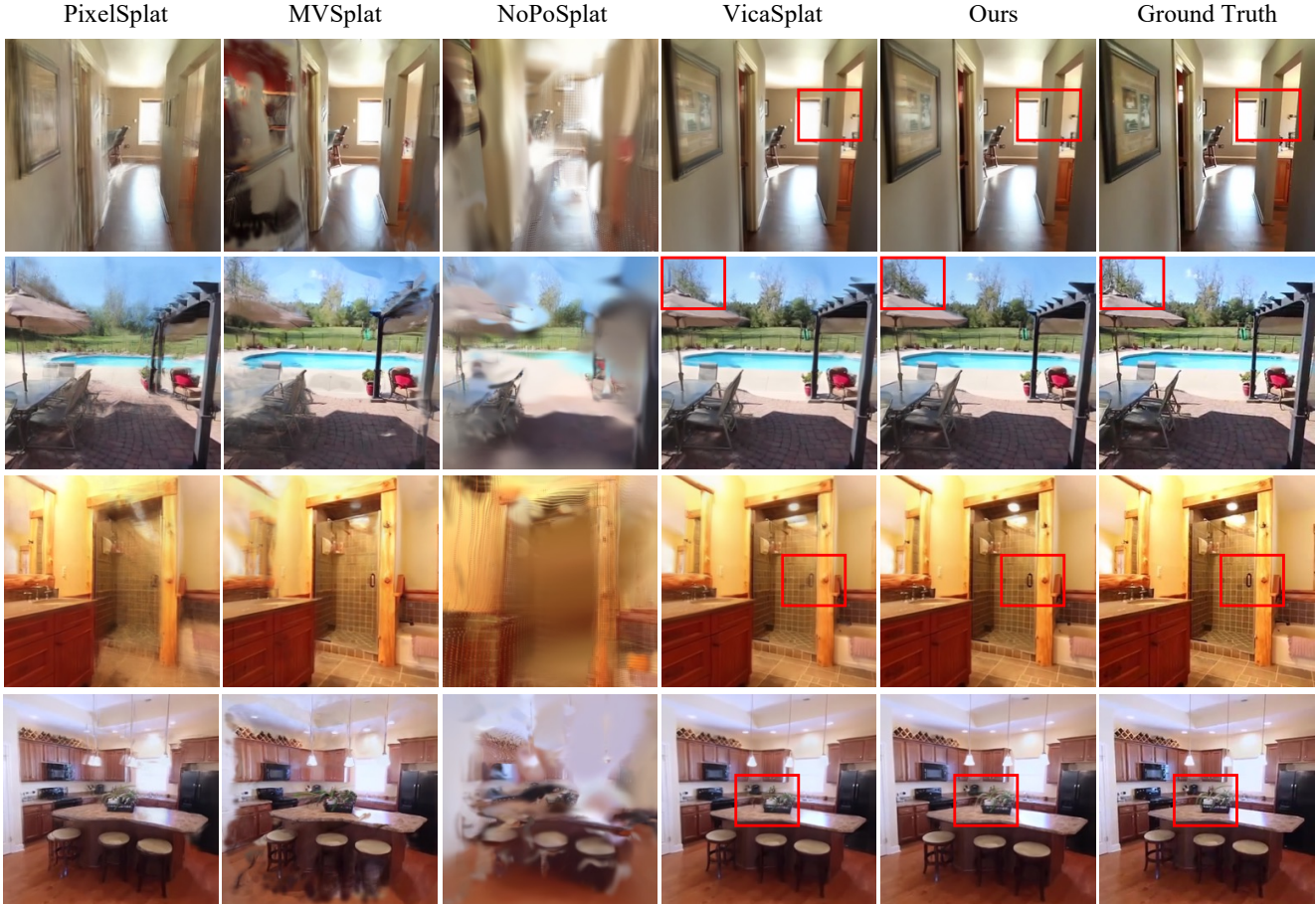


Figure 3. Qualitative comparison of novel view synthesis on RealEstate10k test set with 8 input images.

3.3. Training Objectives

Photometric Loss (\mathcal{L}_{rgb}). To ensure that rendered images match the input views, we combine a pixel-wise L1 loss and the LPIPS metric [44]:

$$\mathcal{L}_{\text{rgb}} = \sum_{i=1}^N \left(\|\tilde{I}^{(i)} - \hat{I}^{(i)}\|_1 + \lambda_{\text{LPIPS}} \text{LPIPS}(\tilde{I}^{(i)}, \hat{I}^{(i)}) \right), \quad (10)$$

where $\tilde{I}^{(i)}$ and $\hat{I}^{(i)}$ denotes the ground-truth image and the rendered image from the i -th camera viewpoint, respectively, and λ_{LPIPS} is set to 0.05.

Semantic Loss (\mathcal{L}_{sem}). To endow the Gaussians with open-vocabulary capabilities, we distill knowledge from a frozen, pre-trained 2D vision-language model, LSeg [18]. We extract feature maps $\tilde{F}^{(i)}$ from each input image using the LSeg image encoder. We then enforce alignment between the rendered semantic feature map $\hat{F}^{(i)'}$ and the 2D CLIP-based features using a cosine similarity loss:

$$\mathcal{L}_{\text{sem}} = \sum_{i=1}^N \left(1 - \frac{\tilde{F}^{(i)} \cdot \hat{F}^{(i)'}}{\|\tilde{F}^{(i)}\| \cdot \|\hat{F}^{(i)'}\|} \right). \quad (11)$$

This loss lifts rich 2D semantics into the 3D domain, enabling zero-shot semantic understanding without requiring explicit 3D annotations.

Geometry Loss (\mathcal{L}_{geo}). To enhance geometric consistency and training stability, we adopt a point-map regularization strategy inspired by PM-Loss [31]. This regularization simultaneously improves structural accuracy—particularly around object boundaries—and mitigates collapse during optimization. Under RGB-only supervision, the model lacks explicit geometric constraints on the predicted point cloud, often leading to local minima and unstable convergence. The introduced point-map constraint provides a strong geometric prior that guides the 3D Gaussian distribution toward both structurally consistent and stable reconstruction. Specifically, we leverage a frozen VGGT [36] to generate a dense point map $\hat{\mu}^{(i)} \in \mathbb{R}^{3 \times H \times W}$ to guide geometric supervision. Given that the predictions from VGGT are not uniformly reliable, especially in challenging regions such as reflective surfaces or areas with heavy occlusion, we introduce a confidence-based masking strategy. We extract the confidence map

Method	Recon. Time↓		Source View				Target View				
	SfM	Per-Scene	mIoU↑	Acc.↑	rel↓	τ ↑	mIoU↑	Acc.↑	PSNR↑	SSIM↑	LPIPS↓
LSeg	N/A	N/A	0.4701	0.7891	-	-	0.4819	0.7927	-	-	-
NeRF-DFD	20.52s	1min	0.4540	0.7173	27.68	9.61	0.4037	0.6755	19.86	0.6650	0.3629
Feature-3DGS	20.52s	18mins	0.4453	0.7276	12.95	21.07	0.4223	0.7174	24.49	0.8132	0.2293
PixelSplat	0.064s	-	-	-	-	-	-	-	24.89	0.8392	0.1641
LSM*	0.108s	-	0.5034	0.7740	3.38	67.77	0.5078	0.7686	24.39	0.8072	0.2506
AnySplat	-	-	-	-	6.35	47.57	-	-	22.08	0.8118	0.2480
Ours	0.162s	-	0.5403	0.8255	3.87	61.37	0.5584	0.8268	25.53	0.8727	0.1380

Table 1. **Quantitative Comparison on ScanNet.** We evaluate performance on novel view synthesis, depth estimation, and open-vocabulary semantic segmentation. (*) **Unlike LSM, Uni3R is trained without any 3D annotations.**

$C^{(i)}$ from VGGT and construct a binary geometry mask, $M^{(i)} \in \{0, 1\}^{H \times W}$ by selecting the top- k most confident pixels (set as 90% in our experiments). The predicted point maps $\mu^{(i)}$ from Uni3R are then aligned with $\hat{\mu}^{(i)}$ via the Umeyama algorithm [35]. Given the masked aligned point clouds $X_U^{(i)} = \mu^{(i)} \odot M^{(i)}$ and $X_V^{(i)} = \hat{\mu}^{(i)} \odot M^{(i)}$, where \odot denotes the element-wise product, a single-directional Chamfer distance is computed. The loss is formulated as:

$$\mathcal{L}_{\text{geo}} = \sum_{i=1}^N \frac{1}{N_{\text{pts}}^{(i)}} \sum_{x \in X_U^{(i)}} \min_{x' \in X_V^{(i)}} \|x - x'\|_2^2 \quad (12)$$

$N_{\text{pts}}^{(i)}$ is the total number of points. The final training objective is a weighted sum of the individual losses:

$$\mathcal{L}_{\text{total}} = \mathcal{L}_{\text{rgb}} + \lambda_{\text{sem}} \mathcal{L}_{\text{sem}} + \lambda_{\text{geo}} \mathcal{L}_{\text{geo}}, \quad (13)$$

where the balancing hyperparameters λ_{sem} and λ_{geo} are set to 0.02 and 0.005, respectively.

4. Experiments

4.1. Experimental Setup

Dataset For evaluating both 3D scene and semantic field reconstruction, our model is trained on a combined dataset of ScanNet++ [41] and ScanNet [6], totaling 1,565 scenes. We evaluate on 40 unseen ScanNet scenes, and further examine the model’s zero-shot generalization on the Mip-NeRF360 [1] dataset.

Furthermore, to assess rendering quality, we train our model on the RealEstate10K [46] and ACID [22] datasets. To evaluate cross-domain generalization, we test our method on the DTU [10] and ScanNet++ [41] benchmarks (see the supplementary material for more details).

Implementation Details We use DINOv2 [26] as the image encoder, with a patch size of 16, and set the Cross-View Transformer layers as $L = 24$. We initialize the encoder and decoder with the weights from the pretrained

VGGT [36], while the remaining intrinsic layer and Gaussian head are randomly initialized. For a fair comparison with the baseline models, we report all quantitative results under 256×256 . Our model is implemented using PyTorch [27]. All experiments are conducted on $8 \times \text{A100}$ GPUs, taking approximately 22 hours for the training of 2 views, with a batch size of 2. Please refer to the supplementary for more details.

4.2. Experiment Results

Semantic 3D Reconstruction As shown in Tab. 1 and Fig. 4, Uni3R establishes a new state of the art across multiple 3D tasks, producing coherent and precise semantic interpretations. While Uni3R is supervised by LSeg, it outperforms by resolving 2D view-dependent ambiguities through 3D spatial fusion. In Fig. 4, LSeg’s 2D predictions are incorrect for the sofa due to local view. Uni3R, however, aggregates features across multiple views into a unified 3D representation. The underlying multi-view geometry acts as a spatial filter that ‘votes out’ inconsistent 2D errors. Thus, Uni3R not only mimics LSeg, but also leverages 3D consistency to produce a denoised, robust semantic prediction. Furthermore, while methods such as LSM require ground-truth point clouds for supervision, Uni3R eliminates this dependency, demonstrating superior practicality and scalability for real-world applications.

Comparison with Per-Scene Optimized Methods To evaluate efficiency and generalization, we compare Uni3R with the per-scene optimized Feature 3DGS [45]. Such methods rely on Structure-from-Motion [7] to estimate camera poses, leading to high computational overhead and poor scalability. In contrast, as shown in Tab. 2 and Tab. 5, Uni3R demonstrates strong generalization by reconstructing consistent 3D geometry, rendering and semantics from unposed multiview inputs. Notably, it achieves superior performance in both novel view synthesis and open-vocabulary segmentation, offering a substantial speed advantage over traditional per-scene optimization methods.

Method	Feed-Forward	8 views							16 views						
		Time↓	PSNR↑	SSIM↑	mIoU↑	Acc.↑	rel↓	τ ↑	Time↓	PSNR↑	SSIM↑	mIoU↑	Acc.↑	rel↓	τ ↑
Feature-3DGS	✗	$\approx 40min$	18.17	0.674	0.195	0.724	17.28	13.31	$\approx 60min$	17.09	0.649	0.198	0.672	23.71	10.57
Ours	✓	0.359s	24.71	0.851	0.554	0.807	4.25	57.41	0.636s	23.32	0.816	0.558	0.835	3.97	60.48

Table 2. Comparison with Per-Scene Optimized Methods. Time corresponds to the average reconstruction time per scene.

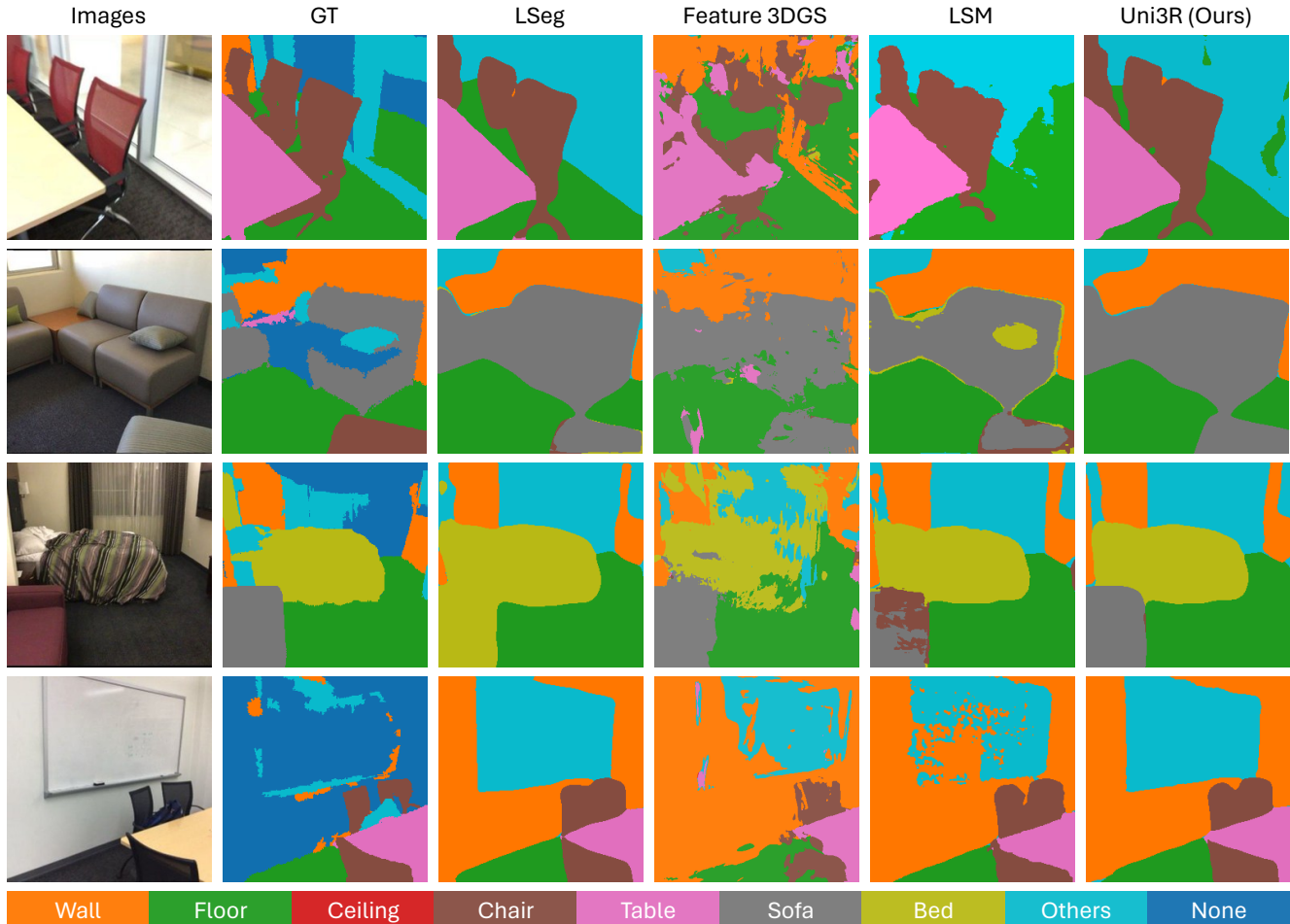


Figure 4. Qualitative Comparison of Novel-View Segmentation on ScanNet.

Method	RE10k			ACID			
	PSNR↑	SSIM↑	LPIPS↓	PSNR↑	SSIM↑	LPIPS↓	
<i>Pose-Required</i>	PixelSplat	23.361	0.803	0.186	25.684	0.778	0.194
	MVSplat	23.430	0.805	0.179	25.335	0.772	0.195
<i>Pose-Free</i>	NoPoSplat	25.036	0.838	0.162	25.961	0.781	0.189
	CoPoNeRF	18.938	0.619	0.388	20.950	0.606	0.406
	VicaSplat	<u>25.038</u>	0.834	<u>0.161</u>	25.439	0.757	0.201
	Ours	25.074	0.837	0.158	<u>25.766</u>	<u>0.778</u>	<u>0.192</u>

Table 3. Quantitative comparisons of novel view synthesis on the RE10k [46] and ACID [22] dataset under 2-views setup.

Novel-View Synthesis As shown in Tab. 3, Uni3R outperforms pose-dependent methods, such as PixelSplat and

MVSplat, by a clear margin (1.7dB), and slightly surpasses baseline model NoPoSplat with a gain of 0.2dB on the RE10k dataset.

Fig. 3 demonstrates Uni3R consistently produces more detailed and structurally coherent constructions. For example, in the Pool Scene, it recovers the forest area with sharper geometry, while VicaSplat shows blurring and discontinuities. These results highlight Uni3R’s ability to preserve fine details and structural consistency in pose-free multi-view 3D reconstruction.

The quantitative results in Tab. 4 further validate the effectiveness of Uni3R in aggregating information across multiple views. Uni3R consistently outperforms all baselines under both 4-view and 8-view settings. Notably, it

Method	4 views (RE10k)			8 views (RE10k)			4 views (ScanNet)			8 views (ScanNet)			
	PSNR \uparrow	SSIM \uparrow	LPIPS \downarrow	PSNR \uparrow	SSIM \uparrow	LPIPS \downarrow	PSNR \uparrow	SSIM \uparrow	LPIPS \downarrow	PSNR \uparrow	SSIM \uparrow	LPIPS \downarrow	
<i>Pose-Required</i>	PixelSplat	20.459	0.729	0.267	19.734	0.694	0.290	21.185	0.712	0.351	18.582	0.637	0.440
	MVSplat	20.882	0.761	0.233	19.726	0.743	0.262	14.946	0.472	0.544	13.061	0.407	0.608
<i>Pose-Free</i>	NoPoSplat	16.299	0.552	0.397	14.372	0.469	0.520	16.940	0.560	0.425	12.939	0.397	0.588
	CoPoNeRF	18.299	0.655	0.559	18.984	0.692	0.553	20.247	0.775	0.535	19.821	0.772	0.542
	VicaSplat	24.537	0.814	0.162	24.502	0.806	0.164	26.673	0.856	0.188	23.656	0.777	0.262
	AnySplat	18.860	0.654	-	20.273	0.602	-	21.075	0.722	-	19.303	0.701	-
	Ours	26.360	0.866	0.129	26.629	0.874	0.118	28.324	0.891	0.161	26.019	0.858	0.193

Table 4. Comparison with 4 and 8-view settings on the RE10k [46] and ScanNet [6] datasets.

Method	2View			8View		
	PSNR \uparrow	SSIM \uparrow	LPIPS \downarrow	PSNR \uparrow	SSIM \uparrow	LPIPS \downarrow
Anysplat [12]	17.329	0.401	0.295	18.805	0.434	0.308
Ours	17.331	0.393	0.283	19.196	0.491	0.355

Table 5. Zero-shot generalization on Mip-NeRF360 [1] dataset

View Num	PSNR \uparrow	SSIM \uparrow	LPIPS \downarrow	mIoU \uparrow	Acc \uparrow	rel \downarrow
2 Views	25.27	0.867	0.141	0.5418	0.8182	4.72
4 Views	25.45	0.845	0.145	0.4018	0.7616	5.76
8 Views	24.76	0.848	0.154	0.5539	0.8184	7.88

Table 6. Arbitrary View model training and evaluation on the ScanNet [6] dataset.

delivers an average improvement of 2.0 dB over VicaSplat [20], a strong sequential baseline designed for unposed video inputs, demonstrating Uni3R’s superior generalization and multi-view integration capabilities. Furthermore, Uni3R surpasses AnySplat [12] on the zero-shot Mip-NeRF360 [1] dataset in Tab. 5 and underscoring its robustness and cross-domain generalization ability.

4.3. Analysis and Ablations

Results on Different Input View Numbers To demonstrate Uni3R’s ability to handle arbitrary view inputs, we report results in Tab. 6. Unlike Vicasplat [20], which focuses solely on sequential rendering, and LSM [8], which reconstructs semantic and radiance fields but is restricted to two-view inputs, Uni3R is the first unified model to jointly reconstruct radiance and semantic fields from unposed multi-view images. This experiment highlights Uni3R’s ability to handle long sequences and wide-baseline configurations, producing high-fidelity and semantically consistent 3D reconstructions in a single feed-forward pass.

Ablation Study on Our Modules We conduct ablation studies on Uni3R to analyze the impact of different supervisory signals and architectural components (see Tab. 7).

Method	mIoU \uparrow	rel \downarrow	τ \uparrow	PSNR \uparrow	SSIM \uparrow
frozen all transformer layers	0.0634	51.1	7.6	5.49	0.052
w/o semantic loss	0.0183	5.8	47.4	25.38	0.869
w/o rendering loss	0.2653	N/A	N/A	N/A	N/A
w/o scale invariant	0.5382	5.8	47.9	24.95	0.861
w/o intrinsic embedding	0.5471	6.5	42.5	25.35	0.871
w/o geo. loss	0.5541	5.6	48.2	25.53	0.872
Ours	0.5484	3.9	61.2	25.53	0.873

Table 7. Ablation Study on different modules. We evaluate the ablated variants of Uni3R, by recording their rendering quality, segmentation performance and geometric accuracy.

Removing the semantic loss causes a severe collapse in segmentation accuracy, underscoring its necessity for open-vocabulary semantic learning. Excluding the rendering loss leads to non-convergence, confirming its critical role in guiding 3D reconstruction. When the geometric loss is removed, the model exhibits degraded 3D consistency (higher depth error and lower τ), validating its effectiveness in improving point cloud distribution and depth alignment. The scale-invariant constraint contributes to rendering stability across scenes with varying depth ranges, while the intrinsic embedding improves robustness by aligning scenes of varying scales into a consistent geometric space. Overall, these results demonstrate that Uni3R’s unified supervision of semantic, radiance, and geometric fields is essential for achieving high-fidelity and semantically consistent 3D reconstruction.

5. Conclusion

Uni3R is a generalizable framework for unified 3D reconstruction and semantic understanding from unposed multi-view images. It predicts a Gaussian-based representation to integrate appearance, geometry, and open-vocabulary semantics in a single forward pass. To address geometric inaccuracies under RGB-only supervision, we introduce a geometry-guided loss to enhance depth consistency. Uni3R takes a significant step toward scalable, multi-view 3D scene understanding for real-world applications, such as autonomous navigation and real-time 3D perception.

References

- [1] Jonathan T Barron, Ben Mildenhall, Dor Verbin, Pratul P Srinivasan, and Peter Hedman. Mip-nerf 360: Unbounded anti-aliased neural radiance fields. In *Proceedings of the IEEE/CVF conference on computer vision and pattern recognition*, pages 5470–5479, 2022. 6, 8
- [2] Michael Bleyer, Christoph Rhemann, and Carsten Rother. Patchmatch stereo - stereo matching with slanted support windows. In *British Machine Vision Conference, BMVC 2011, Dundee, UK, August 29 - September 2, 2011. Proceedings*, pages 1–11, 2011. 2
- [3] David Charatan, Sizhe Lester Li, Andrea Tagliasacchi, and Vincent Sitzmann. Pixelsplat: 3d gaussian splats from image pairs for scalable generalizable 3d reconstruction. In *IEEE/CVF Conference on Computer Vision and Pattern Recognition, CVPR 2024, Seattle, WA, USA, June 16-22, 2024*, pages 19457–19467, 2024. 2
- [4] Anpei Chen, Zexiang Xu, Fuqiang Zhao, Xiaoshuai Zhang, Fanbo Xiang, Jingyi Yu, and Hao Su. Mvsnerf: Fast generalizable radiance field reconstruction from multi-view stereo. In *2021 IEEE/CVF International Conference on Computer Vision, ICCV 2021, Montreal, QC, Canada, October 10-17, 2021*, pages 14104–14113, 2021. 2
- [5] Yuedong Chen, Haofei Xu, Chuanxia Zheng, Bohan Zhuang, Marc Pollefeys, Andreas Geiger, Tat-Jen Cham, and Jianfei Cai. Mvsplat: Efficient 3d gaussian splatting from sparse multi-view images. In *Computer Vision - ECCV 2024 - 18th European Conference, Milan, Italy, September 29-October 4, 2024, Proceedings, Part XXI*, pages 370–386, 2024. 2
- [6] Angela Dai, Angel X. Chang, Manolis Savva, Maciej Halber, Thomas A. Funkhouser, and Matthias Nießner. Scannet: Richly-annotated 3d reconstructions of indoor scenes. In *2017 IEEE Conference on Computer Vision and Pattern Recognition, CVPR 2017, Honolulu, HI, USA, July 21-26, 2017*, pages 2432–2443, 2017. 2, 6, 8, 1
- [7] Frank Dellaert, Steven M. Seitz, Charles E. Thorpe, and Sebastian Thrun. Structure from motion without correspondence. In *2000 Conference on Computer Vision and Pattern Recognition (CVPR 2000), 13-15 June 2000, Hilton Head, SC, USA*, pages 2557–2564, 2000. 2, 6
- [8] Zhiwen Fan, Jian Zhang, Wenyan Cong, Peihao Wang, Renjie Li, Kairun Wen, Shijie Zhou, Achuta Kadambi, Zhangyang Wang, Danfei Xu, Boris Ivanovic, and Marco Pavone. Large spatial model: End-to-end unposed images to semantic 3d. In *Advances in Neural Information Processing Systems 38: Annual Conference on Neural Information Processing Systems 2024, NeurIPS 2024, Vancouver, BC, Canada, December 10 - 15, 2024*, 2024. 2, 3, 8, 1
- [9] Wenhao Hu, Wenhao Chai, Shengyu Hao, Xiaotong Cui, Xuexiang Wen, Jenq-Neng Hwang, and Gaoang Wang. Pointmap association and piecewise-plane constraint for consistent and compact 3d gaussian segmentation field. *arXiv preprint arXiv:2502.16303*, 2025. 2
- [10] Rasmus Ramsbøl Jensen, Anders Lindbjerg Dahl, George Vogiatzis, Engin Tola, and Henrik Aanæs. Large scale multi-view stereopsis evaluation. In *2014 IEEE Conference on Computer Vision and Pattern Recognition, CVPR 2014, Columbus, OH, USA, June 23-28, 2014*, pages 406–413. IEEE Computer Society, 2014. 6, 1
- [11] Haoyi Jiang, Liu Liu, Tianheng Cheng, Xinjie Wang, Tianwei Lin, Zhizhong Su, Wenyu Liu, and Xinggang Wang. Gausstr: Foundation model-aligned gaussian transformer for self-supervised 3d spatial understanding. In *IEEE/CVF Conference on Computer Vision and Pattern Recognition, CVPR 2025, Nashville, TN, USA, June 11-15, 2025*, pages 11960–11970, 2025. 3
- [12] Lihan Jiang, Yucheng Mao, Linning Xu, Tao Lu, Kerui Ren, Yichen Jin, Xudong Xu, Mulin Yu, Jiangmiao Pang, Feng Zhao, et al. Anysplat: Feed-forward 3d gaussian splatting from unconstrained views. *arXiv preprint arXiv:2505.23716*, 2025. 8
- [13] Gyeongjin Kang, Seungtae Nam, Xiangyu Sun, Sameh Khamis, Abdelrahman Mohamed, and Eunbyung Park. ilrm: An iterative large 3d reconstruction model, 2025. 3
- [14] Bernhard Kerbl, Georgios Kopanas, Thomas Leimkühler, and George Drettakis. 3d gaussian splatting for real-time radiance field rendering. *ACM Trans. Graph.*, 42(4):139:1–139:14, 2023. 2
- [15] Justin Kerr, Chung Min Kim, Ken Goldberg, Angjoo Kanazawa, and Matthew Tancik. LERF: language embedded radiance fields. In *IEEE/CVF International Conference on Computer Vision, ICCV 2023, Paris, France, October 1-6, 2023*, pages 19672–19682, 2023. 3
- [16] Joo Chan Lee, Daniel Rho, Xiangyu Sun, Jong Hwan Ko, and Eunbyung Park. Compact 3d gaussian representation for radiance field. In *Proceedings of the IEEE/CVF Conference on Computer Vision and Pattern Recognition*, pages 21719–21728, 2024. 2
- [17] Vincent Leroy, Yohann Cabon, and Jérôme Revaud. Grounding image matching in 3d with mast3r. In *Computer Vision - ECCV 2024 - 18th European Conference, Milan, Italy, September 29-October 4, 2024, Proceedings, Part LXXII*, pages 71–91, 2024. 3
- [18] Boyi Li, Kilian Q. Weinberger, Serge J. Belongie, Vladlen Koltun, and René Ranftl. Language-driven semantic segmentation. In *The Tenth International Conference on Learning Representations, ICLR 2022, Virtual Event, April 25-29, 2022*, 2022. 5
- [19] Yongkang Li, Tianheng Cheng, Bin Feng, Wenyu Liu, and Xinggang Wang. Mask-adapter: The devil is in the masks for open-vocabulary segmentation. In *IEEE/CVF Conference on Computer Vision and Pattern Recognition, CVPR 2025, Nashville, TN, USA, June 11-15, 2025*, pages 14998–15008. Computer Vision Foundation / IEEE, 2025. 3
- [20] Zhiqi Li, Chengrui Dong, Yiming Chen, Zhangchi Huang, and Peidong Liu. Vicasplat: A single run is all you need for 3d gaussian splatting and camera estimation from unposed video frames. *CoRR*, abs/2503.10286, 2025. 8
- [21] Siyun Liang, Sen Wang, Kunyi Li, Michael Niemeyer, Stefano Gasperini, Nassir Navab, and Federico Tombari. Superseg: Open-vocabulary 3d segmentation with structured super-gaussians. *arXiv preprint arXiv:2412.10231*, 2024. 3
- [22] Andrew Liu, Ameer Makadia, Richard Tucker, Noah Snaveley, Varun Jampani, and Angjoo Kanazawa. Infinite na-

- ture: Perpetual view generation of natural scenes from a single image. In *2021 IEEE/CVF International Conference on Computer Vision, ICCV 2021, Montreal, QC, Canada, October 10-17, 2021*, pages 14438–14447. IEEE, 2021. 6, 7, 1
- [23] Tianqi Liu, Guangcong Wang, Shoukang Hu, Liao Shen, Xinyi Ye, Yuhang Zang, Zhiguo Cao, Wei Li, and Ziwei Liu. Mvsgaussian: Fast generalizable gaussian splatting reconstruction from multi-view stereo. In *European Conference on Computer Vision*, pages 37–53. Springer, 2024. 2
- [24] Ben Mildenhall, Pratul P. Srinivasan, Matthew Tancik, Jonathan T. Barron, Ravi Ramamoorthi, and Ren Ng. Nerf: Representing scenes as neural radiance fields for view synthesis. In *Computer Vision - ECCV 2020 - 16th European Conference, Glasgow, UK, August 23-28, 2020, Proceedings, Part I*, pages 405–421, 2020. 2
- [25] Seungtae Nam, Xiangyu Sun, Gyeongjin Kang, Younggeun Lee, Seungjun Oh, and Eunbyung Park. Generative densification: Learning to densify gaussians for high-fidelity generalizable 3d reconstruction. In *IEEE/CVF Conference on Computer Vision and Pattern Recognition, CVPR 2025, Nashville, TN, USA, June 11-15, 2025*, pages 26683–26693. Computer Vision Foundation / IEEE, 2025. 2
- [26] Maxime Oquab, Timothée Darcet, Théo Moutakanni, and Huy V. Vo et al. Dinov2: Learning robust visual features without supervision. *Trans. Mach. Learn. Res.*, 2024. 4, 6
- [27] Adam Paszke, Sam Gross, and Francisco Massa et al. Pytorch: An imperative style, high-performance deep learning library. In *Advances in Neural Information Processing Systems 32: Annual Conference on Neural Information Processing Systems 2019, NeurIPS 2019, December 8-14, 2019, Vancouver, BC, Canada*, pages 8024–8035, 2019. 6
- [28] Minghan Qin, Wanhua Li, Jiawei Zhou, Haoqian Wang, and Hanspeter Pfister. Langsplat: 3d language gaussian splatting. In *IEEE/CVF Conference on Computer Vision and Pattern Recognition, CVPR 2024, Seattle, WA, USA, June 16-22, 2024*, pages 20051–20060, 2024. 2, 3
- [29] Alec Radford, Jong Wook Kim, and Ilya Sutskever et al. Learning transferable visual models from natural language supervision. In *Proceedings of the 38th International Conference on Machine Learning, ICML 2021, 18-24 July 2021, Virtual Event*, pages 8748–8763, 2021. 3
- [30] René Ranftl, Alexey Bochkovskiy, and Vladlen Koltun. Vision transformers for dense prediction. In *2021 IEEE/CVF International Conference on Computer Vision, ICCV 2021, Montreal, QC, Canada, October 10-17, 2021*, pages 12159–12168, 2021. 4
- [31] Duochao Shi, Weijie Wang, Donny Y. Chen, Zeyu Zhang, Jia-Wang Bian, Bohan Zhuang, and Chunhua Shen. Revisiting depth representations for feed-forward 3d gaussian splatting. *CoRR*, abs/2506.05327, 2025. 5
- [32] Brandon Smart, Chuanxia Zheng, Iro Laina, and Victor Adrian Prisacariu. Splatt3r: Zero-shot gaussian splatting from uncalibrated image pairs. *CoRR*, abs/2408.13912, 2024. 3
- [33] Xiangyu Sun, Joo Chan Lee, Daniel Rho, Jong Hwan Ko, Usman Ali, and Eunbyung Park. F-3dgs: Factorized coordinates and representations for 3d gaussian splatting. In *Proceedings of the 32nd ACM International Conference on Multimedia*, pages 7957–7965, 2024. 2
- [34] Qijian Tian, Xin Tan, Jingyu Gong, Yuan Xie, and Lizhuang Ma. Uniforward: Unified 3d scene and semantic field reconstruction via feed-forward gaussian splatting from only sparse-view images. *CoRR*, abs/2506.09378, 2025. 2
- [35] Shinji Umeyama. Least-squares estimation of transformation parameters between two point patterns. *IEEE Trans. Pattern Anal. Mach. Intell.*, 13(4):376–380, 1991. 6
- [36] Jianyuan Wang, Minghao Chen, Nikita Karaev, Andrea Vedaldi, Christian Rupprecht, and David Novotný. VGGT: visual geometry grounded transformer. In *IEEE/CVF Conference on Computer Vision and Pattern Recognition, CVPR 2025, Nashville, TN, USA, June 11-15, 2025*, pages 5294–5306, 2025. 2, 3, 5, 6
- [37] Shuzhe Wang, Vincent Leroy, Yohann Cabon, Boris Chidlovskii, and Jérôme Revaud. Dust3r: Geometric 3d vision made easy. In *IEEE/CVF Conference on Computer Vision and Pattern Recognition, CVPR 2024, Seattle, WA, USA, June 16-22, 2024*, pages 20697–20709, 2024. 2, 3
- [38] Xingrui Wang, Cuiling Lan, Hanxin Zhu, Zhibo Chen, and Yan Lu. Gsemplat: Generalizable semantic 3d gaussian splatting from uncalibrated image pairs. *arXiv preprint arXiv:2412.16932*, 2024. 3
- [39] Haofei Xu, Songyou Peng, and Marc Pollefeys et al. Depthsplat: Connecting gaussian splatting and depth. In *IEEE/CVF Conference on Computer Vision and Pattern Recognition, CVPR 2025, Nashville, TN, USA, June 11-15, 2025*, pages 16453–16463. Computer Vision Foundation / IEEE, 2025. 2, 3
- [40] Botao Ye, Sifei Liu, Haofei Xu, Xueting Li, Marc Pollefeys, Ming-Hsuan Yang, and Songyou Peng. No pose, no problem: Surprisingly simple 3d gaussian splats from sparse unposed images. In *The Thirteenth International Conference on Learning Representations, ICLR 2025, Singapore, April 24-28, 2025*. 3, 4, 1
- [41] Chandan Yeshwanth, Yueh-Cheng Liu, Matthias Nießner, and Angela Dai. Scannet++: A high-fidelity dataset of 3d indoor scenes. In *IEEE/CVF International Conference on Computer Vision, ICCV 2023, Paris, France, October 1-6, 2023*, pages 12–22. IEEE, 2023. 6, 1
- [42] Alex Yu, Vickie Ye, Matthew Tancik, and Angjoo Kanazawa. pixelnerf: Neural radiance fields from one or few images. In *IEEE Conference on Computer Vision and Pattern Recognition, CVPR 2021, virtual, June 19-25, 2021*, pages 4578–4587, 2021. 2
- [43] Hongjia Zhai, Hai Li, Zhenzhe Li, Xiaokun Pan, Yijia He, and Guofeng Zhang. Panogs: Gaussian-based panoptic segmentation for 3d open vocabulary scene understanding. In *Proceedings of the Computer Vision and Pattern Recognition Conference*, pages 14114–14124, 2025. 3
- [44] Richard Zhang, Phillip Isola, Alexei A. Efros, Eli Shechtman, and Oliver Wang. The unreasonable effectiveness of deep features as a perceptual metric. In *2018 IEEE Conference on Computer Vision and Pattern Recognition, CVPR 2018, Salt Lake City, UT, USA, June 18-22, 2018*, pages 586–595. Computer Vision Foundation / IEEE Computer Society, 2018. 5

- [45] Shijie Zhou, Haoran Chang, Sicheng Jiang, Zhiwen Fan, Zehao Zhu, Dejie Xu, Pradyumna Chari, Suyu You, Zhangyang Wang, and Achuta Kadambi. Feature 3dgs: Supercharging 3d gaussian splatting to enable distilled feature fields. In *IEEE/CVF Conference on Computer Vision and Pattern Recognition, CVPR 2024, Seattle, WA, USA, June 16-22, 2024*, pages 21676–21685, 2024. [2](#), [3](#), [6](#), [1](#)
- [46] Tinghui Zhou, Richard Tucker, John Flynn, Graham Fyffe, and Noah Snavely. Stereo magnification: Learning view synthesis using multiplane images. *arXiv preprint arXiv:1805.09817*, 2018. [2](#), [6](#), [7](#), [8](#), [1](#)

Uni3R: Unified 3D Reconstruction and Semantic Understanding via Generalizable Gaussian Splatting from Unposed Multi-View Images

Supplementary Material

Table 8. **Out-of-distribution performance comparison.** Our method shows superior performance when zero-shot evaluation on DTU and ScanNet++ using the model solely trained on RE10k.

Method	DTU		ScanNet++	
	PSNR \uparrow	LPIPS \downarrow	PSNR \uparrow	LPIPS \downarrow
pixelSplat	11.551	0.633	18.434	0.277
MVSplat	13.929	0.385	17.125	0.297
NoPoSplat	17.899	0.279	22.136	0.232
Ours	18.256	0.266	22.221	0.227

Table 9. Ablation Study for confidence mask ratio (top-K) on the ScanNet dataset under 2-views setup on source views.

Top-k ratio mask	mIoU \uparrow	Acc. \uparrow	rel \downarrow	τ \uparrow	PSNR \uparrow	SSIM \uparrow	LPIPS \downarrow
w/o geo. loss	53.88	82.18	5.81	47.99	24.24	0.850	0.108
w/ ratio 100%	53.86	82.46	3.92	60.75	24.24	0.851	0.108
w/ ratio 90%	54.03	82.55	3.87	61.37	24.35	0.851	0.107
w/ ratio 70%	54.00	82.47	4.55	55.28	24.17	0.848	0.111

6. Appendix

6.1. Results on the DTU and ScanNet++ dataset

To evaluate the cross-domain generalization of Uni3R, we follow NoPoSplat [40]: training on RE10K [46] dataset and testing on DTU [10] and ScanNet++[41] dataset. As shown in Tab. 8, Uni3R consistently outperforms all baseline methods on the benchmarks.

6.2. More Ablation Study on confidence parameter setting in geometry-guided loss

To validate the effectiveness of our confidence mask in geometry-guided loss, we conduct an ablation study by varying the top-K ratio used for supervision. As shown in Table 9, applying a 90% confidence mask yields the best performance in mIoU, depth accuracy, and rendering quality, demonstrating that filtering out low-confidence regions improves overall performance.

Furthermore, the geo. loss from the point map is an essential stability anchor for our unified tasks. In Fig. 5, training without this constraint under complex setups (e.g., 4-view) leads to model collapse due to the high degree of freedom in Gaussian optimization. Furthermore, Tab. 9 shows in 2-view, the geometry loss significantly improves geometric (47.99 \rightarrow 61.37) while simultaneously improving mIoU (53.88 \rightarrow 54.03). We believe that observing performance

Figure 5. **Model training w/ and w/o geo. loss on 4 views.**

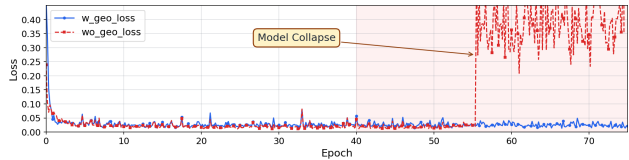


Table 10. **Comparison of our method against per-scene optimized methods.**

Method	8 views		16 views	
	rel \downarrow	τ \uparrow	rel \downarrow	τ \uparrow
Feature-3DGS [45]	17.28	13.31	23.71	10.57
Ours	4.46	56.88	5.88	42.88

improvements across three distinct tasks using only a geometric loss provides a non-trivial insight for the field.

6.3. Depth Evaluation under Multi-View Settings

For fair comparison, we follow LSM [8] and adopt Absolute Relative Error (rel) and Inlier Ratio (τ) with a threshold of 1.03 for per-scene depth evaluation. This setting is consistently used throughout the paper.

As shown in Tab. 10, Uni3R outperforms the per-scene optimized method on depth estimation under both 8-view and 16-view settings. Notably, our method achieves better depth evaluation performance in one feed-forward.

6.4. Training and Evaluation Details

As described in our main paper, we trained our model on three datasets including ScanNet [6], RE10k [46] and ACID [22].

For model training on ACID [22] and RE10K [46] dataset, we progressively train 2, 4 and 8 view model. For 2-view training on ACID [22] and RE10K [46], we follow NoPoSplat [40]. For 4-view training on RE10K, we initialize the model from the 2-view checkpoint and train it on 8xH100 GPUs with a learning rate of 4e-5 for 40,000 iterations, using a batch size of 4 per GPU. For 8-view training, we further initialize from the 4-view checkpoint and train under the same settings, with a batch size of 1 per GPU.

For the ScanNet [6] dataset, we train Uni3R under 2-view, 8-view, and 16-view settings. For the 2-view setup, we follow the LSM [8]. For the 8-view training, we initial-

ize from the 2-view checkpoint and train the model with a learning rate of $5e-5$, with a 5 epochs warmup and 50 total epochs. The batch size is set to 4 per GPU. For the 16-view training, we also initialize from the 2-view checkpoint, with all settings identical to the 8-view setup except for the batch size 2 per GPU.

Additionally, for our arbitrary-view model in the main paper, we uniformly sample 2, 4, and 8 input views from the ScanNet [6] dataset and train the model using a batch size of 1 per GPU. The training is performed with a learning rate of $1e-4$, including a 10-epoch warm-up and 100 total epochs. As demonstrated in the main paper, our arbitrary-view model achieves consistently comparable performance across different numbers of input views.